

Plant infection by the necrotrophic fungus Botrytis requires actin-dependent generation of high invasive turgor pressure

Tobias Müller¹, Jochem Bronkhorst², Jonas Müller¹, Nassim Safari¹, Matthias Hahn¹, Joris Sprakel² (D) and David Scheuring¹ (D)

¹Plant Pathology, Department of Biology, University of Kaiserslautern-Landau, 67663, Kaiserslautern, Germany; ²Green Mechanobiology, Laboratory of Biochemistry, Wageningen University & Research, Stippeneng 4, 6708 WE, Wageningen, the Netherlands

Author for correspondence: David Scheuring

Email: scheuring@bio.uni-kl.de

Received: 15 February 2024 Accepted: 15 July 2024

New Phytologist (2024) 244: 192-201

doi: 10.1111/nph.20025

Key words: appressorium, Botrytis, invasive force, microscopy, pathogens, turgor pressure, virulence.

Summary

- The devastating pathogen Botrytis cinerea infects a broad spectrum of host plants, causing great socio-economic losses. The necrotrophic fungus rapidly kills plant cells, nourishing their wall and cellular contents. To this end, necrotrophs secrete a cocktail of cell wall degrading enzymes, phytotoxic proteins and metabolites. Additionally, many fungi produce specialized invasion organs that generate high invasive pressures to force their way into the plant cell. However, for most necrotrophs, including Botrytis, the biomechanics of penetration and its contribution to virulence are poorly understood.
- Here, we use a combination of quantitative micromechanical imaging and CRISPR—Casguided mutagenesis to show that Botrytis uses substantial invasive pressure, in combination with strong surface adherence, for penetration.
- We found that the fungus establishes a unique mechanical geometry of penetration that develops over time during penetration events, and which is actin cytoskeleton dependent. Furthermore, interference of force generation by blocking actin polymerization was found to decrease Botrytis virulence, indicating that also for necrotrophs, mechanical pressure is important in host colonization.
- Our results demonstrate for the first time mechanistically how a necrotrophic fungus such as Botrytis employs this 'brute force' approach, in addition to the secretion of lytic proteins and phytotoxic metabolites, to overcome plant host resistance.

Introduction

Plant pathogens need to overcome preformed host barriers such as the cuticle and the cell wall for successful host invasion. Unless natural openings such as stomata or wounding can be exploited, pathogens have to create penetration sites. To this end, they can use polymer degrading enzymes, physical force or a combination of both (Hématy et al., 2009). The necrotrophic fungus Botrytis cinerea (Botrytis hereafter) belongs to the economically most devastating pathogens, causing grey mould on numerous vegetables, fruits and other crop plants (Elad, 2007). Successful infection of necrotrophs is characterized by rapid killing of plant cells and depends on the secretion of cutin and cell wall degrading enzymes, and cytolytic and phytotoxic proteins (Bi et al., 2022). While these proteins act redundantly and together are crucial for Botrytis virulence (Leisen et al., 2022), the role of physical force for infection success is poorly understood.

In contrast to necrotrophs, biotrophic pathogens secrete very few lytic enzymes and usually rely on the establishment of specialized infection structures (Mendgen & Deising, 1993; Talbot, 2019) to invade their host cells, causing only limited damage (Mendgen & Hahn, 2002). Infection structures include

appressoria, penetration hyphae, infection hyphae and haustoria, which grow inside plant tissue. Originally, melanin impregnation of the appressorium wall was believed to be critical to generate forces high enough to penetrate plant cell walls. The highly specialized appressorium of Magnaporthe oryzae, and to a lesser extent Colletotrichum graminicola, allow the generation of remarkably high maximal turgor pressures. For mature Magnaporthe grisea appressoria, a turgor pressure of 80 bar has been estimated (Money, 1995), and optical measurements of indentations on artificial substrates by C. graminicola revealed pressures up to 53.5 bar (Bechinger et al., 1999). The belief that such force-based penetration is dependent on melanin-fortified appressoria has been challenged by the observation of an osmotic pressure of 51.3 bar exerted by appressoria of the Asian soybean rust *Phakop*sora pachyrhizi which do not contain melanin (Loehrer et al., 2014). Recently, pressures up to 28 bar were measured in the oomycete *Phytophthora infestans* even without the formation of an visible appressorium (Bronkhorst et al., 2021).

In general, infection structures of necrotrophs are less specialized than those of biotrophs. The Botrytis appressorium lacks distinct morphological features and consists mainly of a terminal thickening of the hyphal tip. However, already in 1895 it

was described that hyphae of Botrytis were able to penetrate gold-coated foils (Miyoshi, 1895); as these are inert to the secreted lytic cocktail, this implies that also this necrotroph is capable of generating significant invasive pressures. To our knowledge, however, neither a quantitative description of turgor pressure generation nor a description of penetration mechanics has been reported for Botrytis or other necrotrophs. The best understood appressorium-mediated penetration process yet is based on research of M. oryzae. Appressorium formation requires the interaction of conserved small GTPases (septins) with actin filaments and microtubules at the appressorium base (Dulal et al., 2020). Here, septins and actin form a ring-like structure of c. 5 µm diameter which lacks melanin and thickened cell wall, allowing osmotic pressure to be channelled towards the emerging penetration peg (Dulal et al., 2021). It has been reported that in septin deletion mutants, actin filaments fail to organize at the appressorium pore, thus preventing the formation of a penetration peg, rendering the mutants nonpathogenic (for an overview refer to Eisermann et al., 2023). Although conserved in filamentous fungi, neither the participation of septins nor a role of the actin cytoskeleton in appressorium formation of Botrytis has been demonstrated

Here, we show that the necrotrophic fungus *Botrytis* employs unique spatio-temporal penetration mechanics. During subsequent stages of penetration, fungal hyphae are raising above incipient appressoria leading to an almost perpendicular entrance angle. In conjunction, the geometry of the adhesive site, that glues the appressorium to the host surface, changes from polarized to nearly isotropic. Moreover, measurements of the penetration kinetics and turgor pressure reveal that the invasive pressure grows up to 5 bar, while the maximally generated turgor pressure is > 40 bar. Finally, we provide evidence that generation of turgor pressure is dependent on the actin skeleton and is required for full virulence of the necrotroph *Botrytis*.

Materials and Methods

Cultivation of Botrytis and infection tests

Botrytis cinerea B05.10 was used as wild-type (WT) strain for infection tests and penetration tests on polydimethylsiloxane (PDMS). To allow for 3D modelling of Botrytis, the fluorescent marker strain Bcgfp1 was employed (Leroch et al., 2011). For the visualization of the actin cytoskeleton, Lifeact-GFP was used (Schumacher, 2012). Cultivation of Botrytis was performed as described previously (Müller et al., 2018). Infection tests on tomato leaflets (Solanum lycopersicum L., variety 'marmonde') were carried out using 1×10^5 spores ml⁻¹ in Gamborg medium with 10 mM glucose. Resulting lesions were documented at defined timepoints (48 and 72 h), and inoculation droplet size and lesion size were quantified (area) using the freehand tool in IMAGEJ. Lesion minus droplet size results in secondary lesion size which we used to calculate the ratio between compared strains. The relative infection was calculated based on B05.10 WT set to 100%.

Penetration on PDMS-coated coverslips

Harvested *Botrytis* conidiospores were diluted to a concentration of 1×10^5 spores ml⁻¹ in Gamborg medium with 10 mM glucose. Eighty microlitre droplets were put in the centre of each coated coverslip. Polydimethylsiloxane was stained with perylene orange and penetration events were analysed after 6, 10, 12, 14 and 18 h using a confocal laser-scanning microscope. This has been done on glass simultaneously.

Plant materials and growth conditions

For infection tests, tomato plants were grown for 4–6 wk on soil in long-day conditions (14 h:10 h, light:dark) at 23°C. The *Arabidopsis thaliana* L. Heynh. spRFP-AFVY marker line (Hunter *et al.*, 2007) for the vacuolar lumen was grown under a long-day regime (16 h:8 h, light:dark) for 4 wk at 22°C before infection.

Confocal microscopy

Images were acquired using a Zeiss LSM880 AxioObserver confocal laser-scanning microscope equipped with a Zeiss C-Apochromat $40\times/1.2$ W AutoCorr M27 water-immersion objective (INST 248/254-1). Fluorescent signals of GFP (excitation/emission 488 nm/500–571 nm) and fluorescent signals of perylene orange (excitation/emission 594 nm/598–696 nm) were processed using the Zeiss software zen 2.3 or ImageJ (https://imagej.nih.gov/ij/). For pressure measurements, z-stacks with 0.5 µm intervals and a resolution of 512×512 pixels were recorded. The z-stacks for 3D surface rendering were recorded with 0.2 µm and a resolution of 1024×1024 pixels.

Surface deformation mapping

Surface deformation maps were reconstructed from the three-dimensional image stacks of the fluorescent PDMS following the procedure described elsewhere (Bronkhorst et al., 2021). In brief: xy-pixels were binned in 2×2 voxels; for each voxel, the intensity profile in the z-direction was fitted to a sigmoidal function to determine the z-position of the PDMS-medium interface with sub-pixel accuracy; the resulting image was finally detilted to remove small tilt angles inherent to sample placement on the microscope table. From these data, for each invasion site, the depth d and radius R of the indentation zone were extracted. By assuming a Hertzian indentation model for a hemisphere indenting a half-space, the Indentation force F is calculated with:

$$F = \frac{4}{3} E R^{\frac{1}{2}} d^{\frac{3}{2}}$$

where E is the effective elastic modulus. For the surfaces used here, this was determined previously to be 6 bar (Bronkhorst *et al.*, 2021), from which in turn the maximum pressure at the invasive site is computed as:

$$P = \frac{1}{\pi} \left(\frac{6FE}{R^2} \right)^{\frac{1}{3}}$$

3D surface rendering

Surface rendering for the reconstruction of *Botrytis* cells and dyed PDMS was performed with IMARIS v.8.4 (Bitplane) software (https://imaris.oxinst.com/). For the creation of models, the surface creation tool was used for the red channel (PDMS) and the green channel (*Bcgfp1*) separately. The generated 3D models were used for angle measurements. To observe individual penetration events on Arabidopsis marker line spRFP-AFVY, 5×10^4 *Bcgfp1* spores/ml in Gamborg medium with 10 mM glucose were incubated on detached leaves for 40–44 h using 5 µl droplets.

Chemicals and treatments

Latrunculin B (Sigma-Aldrich) was used in germination/penetration tests on PDMS and added 10 h after preparing the samples. For infection tests, it was added to the Gamborg medium with 10 mM glucose immediately. Oryzalin (Sigma-Aldrich) was used similarly. It was obtained in powder form and dissolved in DMSO. FITC-labelled concanavalin A (Sigma-Aldrich) was used to stain the connection between *Botrytis* hyphae and PDMS. It was obtained in powder form and dissolved in 0.9% NaCl solution.

Generation of knockout mutants by CRISPR/Cas9

Generation of the multifold (18x) Botrytis gene knockout mutant (Supporting Information Table S1) was carried out as described previously and is based on the established 12-fold mutant (12×bb) (Leisen et al., 2020). In brief, sgRNAs were chosen the web tools CRISPick (https://portals.broadinstitute.org/gppx/ crispick/public) and CHOPCHOP (https://chopchop.cbu.uib. no/). Primers were designed to amplify the respective gDNA and translated to gRNA using the HiScribe T7 High Yield RNA Synthesis Kit (NEB) and purified using the RNA Clean & Concentrator-25 kit (Zymo Research, Orange, CA, USA). All used gRNAs are listed in Table S2. For the formation of ribonucleoprotein (RNP) complexes, 6 µg Cas9-Stu^{2×} protein was incubated with 2 µg sgRNA in cleavage buffer (20 mM HEPES, pH 7.5, 100 mM KCl, 5% glycerol, 1 mM dithiothreitol, 0.5 mM EDTA, pH 8.0 and 2 mM MgCl₂) for 60 min at 37°C. Two RNP complexes were used to target each gene. For the CRISPR/Cas9 editing procedure, 2×10^7 Botrytis protoplasts were transformed with up to four RNPs and 10 µg of pTEL-Fen for selection (Leisen et al., 2022).

Software

Statistical analysis was carried out using the GraphPad Prism 9 software (https://www.graphpad.com/scientific-software/prism/). The detailed statistical method employed is provided in the respective figure legends. Figures were assembled using CorelDRAW v.2021. Figs (3a) and (4d) were generated by using the 'Biorender' software.

Results

To determine the biomechanical behaviour of Botrytis during penetration, we used fluorescently labelled PDMS in combination with confocal laser-scanning microscopy. PDMS represents an artificial substrate resembling in stiffness and hydrophobicity a plant leaf (Bronkhorst et al., 2021), and confocal microscopy allows to follow penetration in depth (z-direction). Initially, Botrytis conidia were inoculated on PDMS-coated coverslips and penetration was observed after 12 h of incubation. We found that Botrytis development on PDMS occurs in a manner similar to that on glass (Fig. S1), involving germination of conidia, appressorium formation and initiation of penetration. Maximum projections of acquired z-stacks reveal a clear displacement of fluorescently labelled PDMS under the appressoria, indicating successful penetration (Fig. 1a). Notably, thinner hyphae emerge from appressoria, resembling penetration hyphae (Fig. S2). For further investigation, we used the previously established fluorescent Botrytis strain Bcgfp1 (Leroch et al., 2011), which allowed generation of 3D-reconstructions (Fig. 1b). By this, we are also able to visualize and quantify indentations of the PDMS layer (Fig. 1c). Comparison of WT *Botrytis* and *Bcgfp1* revealed similar plant infection behaviour, indicating that GFP-expression does not affect virulence (Fig. S3). To compare fungal penetration on PDMS with that on planta, we generated 3D models of Bcgfp1 invading Arabidopsis. To highlight plant epidermal cells, we used the marker line for the vacuolar lumen spRFP-AFVY (Hunter et al., 2007), since in this cell type, up to 90% of the volume is occupied by the vacuole. Penetration patterns were found to be diverse; however, individual penetration events resembled those observed on PDMS (Fig. 1d).

To follow progressive stages of penetration on PDMS, we recorded z-stacks after defined time points and rendered representative 3D models (Fig. 2a-d). Here, we could observe a unique pattern of penetration: Beginning c. 10 h after inoculation, indentations of PDMS were observed, and the hyphal tip was penetrating in an angle which changed during the penetration process. It was initially reminiscent of the so-called naifu penetration (Fig. 2a) observed for Phytophthora (Bronkhorst et al., 2021) but changed later on (Fig. 2b). After 14 h, and more clearly after 18 h, the penetration angle became more perpendicular in parallel with deeper indentations (Fig. 2c,d). Furthermore, we observed increased arching of the hypha close to the appressorium resulting in a visible hunch after 18 h (Fig. 2d). Based on the generated 3D models, we estimated the penetration angles during different stages. Quantification revealed a significant shift from c. 42° to 67° (Fig. 2e,f).

Next, we quantified the substrate deformations induced by the indentation pressure of the *Botrytis* hypha. To this end, *z*-stacks that spanned *c*. 20 µm in the *z*-direction and an axial resolution of 0.5 µm were generated starting at the boundary layer of PMDS and air (Fig. 3a). To capture conidia contact sites and to follow penetration, 20 *z*-slices were recorded above and below the boundary point (Fig. 3a). From the generated stacks, we measured the intensity profile across the substrate—medium interface in each pixel. Fitting these intensity profiles to a sigmoidal

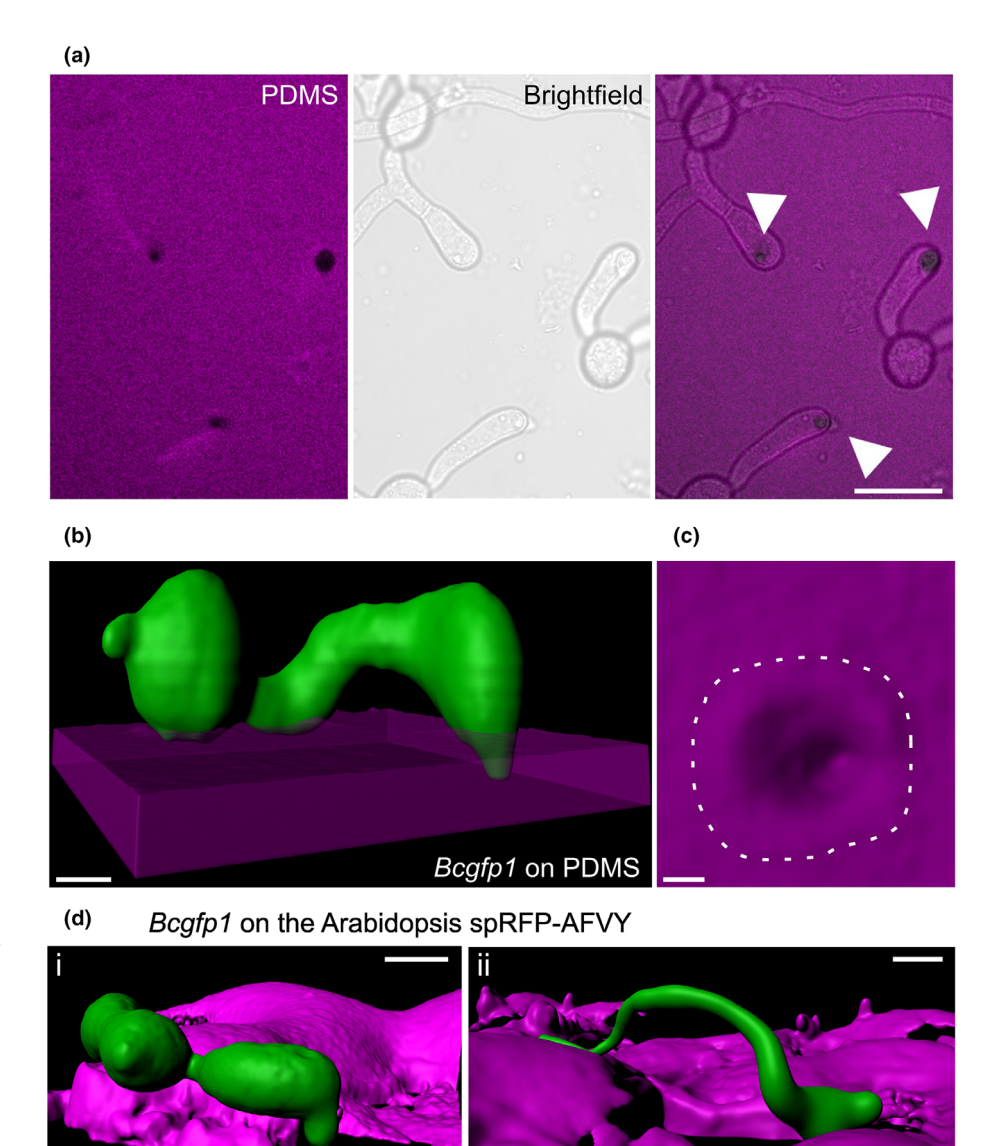


Fig. 1 Development of *Botrytis* conidia on fluorescently labelled polydimethylsiloxane (PDMS). (a) Maximum projection, bright field and merged image of *Botrytis* on PDMS-coated coverslips. Arrowheads indicate appressoria. Bar, 10 μm. (b) 3D model (Imaris) of a spore from the GFP-expressing strain *Bcgfp1* on PDMS after 12 h. Bar, 3 μm. (c) 3D model of surface indentation. Bar, 1 μm. (d) *Botrytis Bcgfp1* penetration *on planta*, using the *Arabidopsis* marker line spRFP-AFVY. Penetration shortly after germination (i) or with bulging hypha (ii). Bars, 10 μm.

function, we could extract surface height Δh (Fig. S4) to display surface deformation maps (Fig. 3b,c). In general, we observed zones of adherence (upward deformations) around the hyphae and indentation (downward deformations) beneath the centre of the appressoria. Earlier time points display a polarized mechanical geometry (Fig. 3b), which is followed by a more concentric circular symmetry later (Fig. 3c). Zones of adherence were positive for concanavalin A (a lectin binding glucosyl and manosyl groups), indicating that carbohydrates binding might allow *Botrytis* to attach to the (artificial) surface (Fig. S5).

In walled cells, the invasive pressure, that is the pressure applied by the pathogen at the penetration site, is generated by the focussing of the internal cellular turgor pressure to a distinct site. To calculate the invasive pressure, we extracted from the surface deformation maps (Fig. 3) for each penetration site both the depth and width of the indentation site. Assuming a Hertzian contact law, and having previously determined the stiffness of the artificial substrate (Bronkhorst *et al.*, 2021), this allows us to calculate the indentation pressure generated by the pathogen at the

invasion site. After 10 h, we found an invasive pressure of 3.7 bar, which was steadily increasing during penetration until it reached 5.0 bar after 18 h (Fig. 3d). For *Phytophthora*, it has been shown that the local invasive pressure accounts only for *c*. 10–20% of the maximal cellular turgor (Bronkhorst *et al.*, 2021). To determine the maximum turgor pressure, we increased the osmotic pressure Π of the medium until suppression of penetration by *Botrytis* was almost complete (Money, 1989; Fig. 3e). This was only reached at osmotic pressures between 27 and 42 bar (Howard *et al.*, 1991) confirming that also for *Botrytis* only 10–20% of the maximum turgor pressure is converted into locally applied, invasive pressure (Fig. 3f).

Since it has been reported that rearrangements of the actin cytos-keleton are a prerequisite for host penetration of *Phytophthora* (Bronkhorst *et al.*, 2022), we asked whether actin has a similar role during *Botrytis* penetration. To interfere with actin filament polymerization, we used the toxin Latrunculin B (LatB) at 500 nM and 1 μ M concentration. Latrunculin has been shown to block actin polymerization in most eukaryotic organisms including fungi

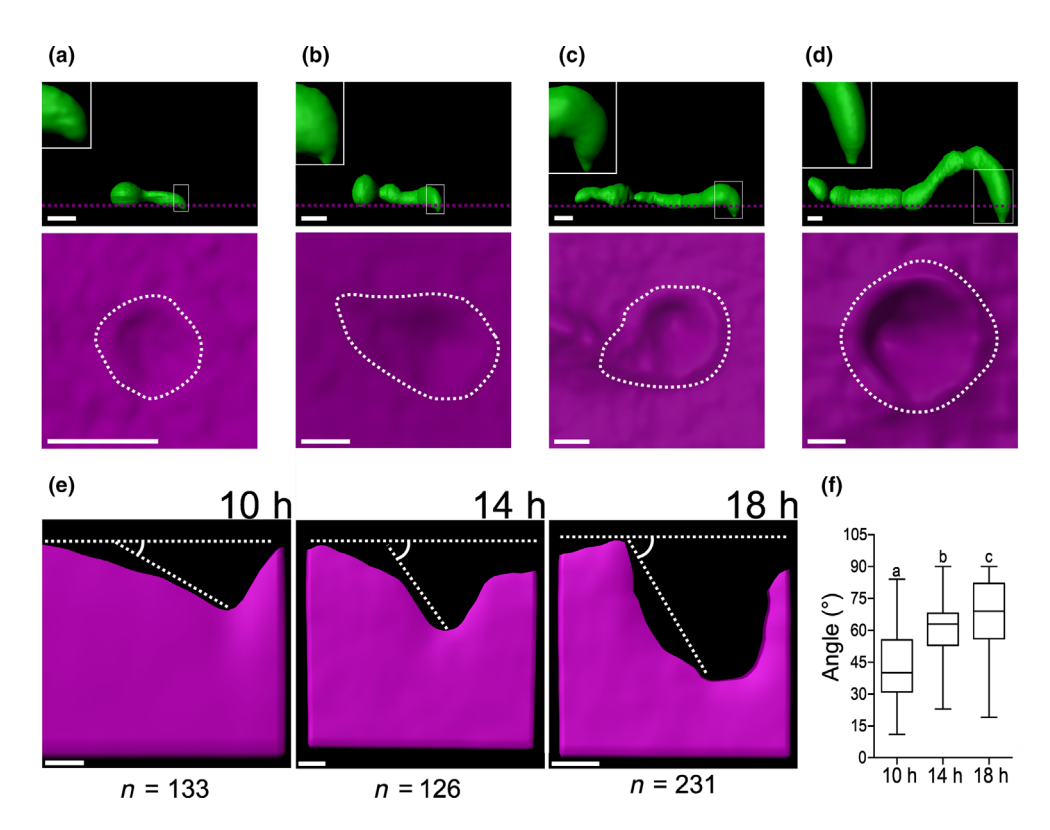


Fig. 2 Kinetics of *Botrytis* penetration reveals a unique pattern. (a–d) Penetration kinetics of fluorescent *Botrytis Bcgfp1* on polydimethylsiloxane (PDMS)-coated coverslips after 6 h (a), 10 h (b), 14 h (c) and 18 h (d). Top part shows a side view of the elevation of a penetrating spore, the inserts showing close-ups of the penetrating tip. Bars: (a–c) 5 μm; (d) 3 μm. Below (in magenta) indentations of PDMS are shown. Bars: (a) 1 μm; (b–d) 3 μm. (e) Penetration angles after 10 h (n = 133), 14 h (n = 126) and 18 h (n = 231). Dotted lines show the measured angle between surface and the tip of the penetration hypha. Bars, 2 μm. (f) Box plot showing the measured angles at each time point. Box limits represent the 25th–75th percentile, the horizontal line the median and the whiskers minimum to maximum values. Statistical differences were analysed by one-way ANOVA with the Tukey *post hoc* test, letters indicating significant differences; P < 0.01. Raw data are found in Supporting Information Table S3. Experiments were repeated twice with similar results; representative models are shown.

(Coué et al., 1987; Ketelaar et al., 2012). Germination was unaffected within this range and a strong growth reduction was only visible at 3 µM LatB (Fig. S6). However, the penetration frequency and depth were visibly suppressed already with 1 µM LatB (Fig. 4a). In addition, we observed structural changes of appressoria when treated with LatB (Fig. 4a, insert). This is somewhat reminiscent of hyphal blunting described for Latrunculin-treated Phytophthora during naifu invasion (Bronkhorst et al., 2022). To investigate the participation of microtubules during the penetration process, we used the microtubule-inhibitor oryzalin. Although most commonly used as a plant-specific inhibitor, oryzalin was shown to be interfering with fungal processes as well, including changes in vacuolar morphology in *Pisolithus tinctorius* and conidial anastomosis tube (CAT)-mediated cell fusion in Verticillium dahliae (Hyde et al., 1999; Vangalis et al., 2021). Therefore, we used oryzalin concentrations up to 100 µM and quantified germination, germ tube length and virulence. While germination was not affected, germ tube length was significantly reduced starting with 10 µM oryzalin but notably no effect on virulence could be observed (Fig. S7).

Delving deeper into the role of actin during appressoria formation, we used the previously established *Botrytis* marker strain Lifeact-GFP (Schumacher, 2012) for visualization of actin filaments. Accumulation of the fusion protein was observed at sites

of septum formation and active tip growth, displaying actin patches and filaments (Fig. 4b). During appressorium formation, filamentous signals condensed and followed a semi-circular or circular distribution connecting patches with filaments (Fig. 4b, c). However, 1 μ M LatB treatment not only reduced filamentous actin as expected but also the general GFP signal intensity decreased (Fig. 4b,c).

Our data with the Lifeact-GFP-expressing strain demonstrated that correct actin filament organization is involved in the formation of appressoria. To clarify whether it is necessary for plant infection, we pharmacologically interfered with actin filament polymerization. To this end, we infected plants in the presence of LatB. Application of 1 μ M LatB caused a significant reduction in lesion formation (Fig. 4d), indicating a disturbed actin cytoskeleton organization and malfunction of the appressorium.

During infection, *Botrytis* secretes a plethora of cutinases, cell wall degrading enzymes and cytolytic proteins to weaken preformed barriers (Bi *et al.*, 2022). It has been therefore assumed that necrotrophic fungi do not rely on the generation of high turgor pressure to breach into the plant cell. To elaborate on the role of turgor formation for infection, we used a multifold *Botrytis* mutant, lacking 18 important phytotoxic secreted proteins and metabolites (Tables S1, S2). This mutant is based on the

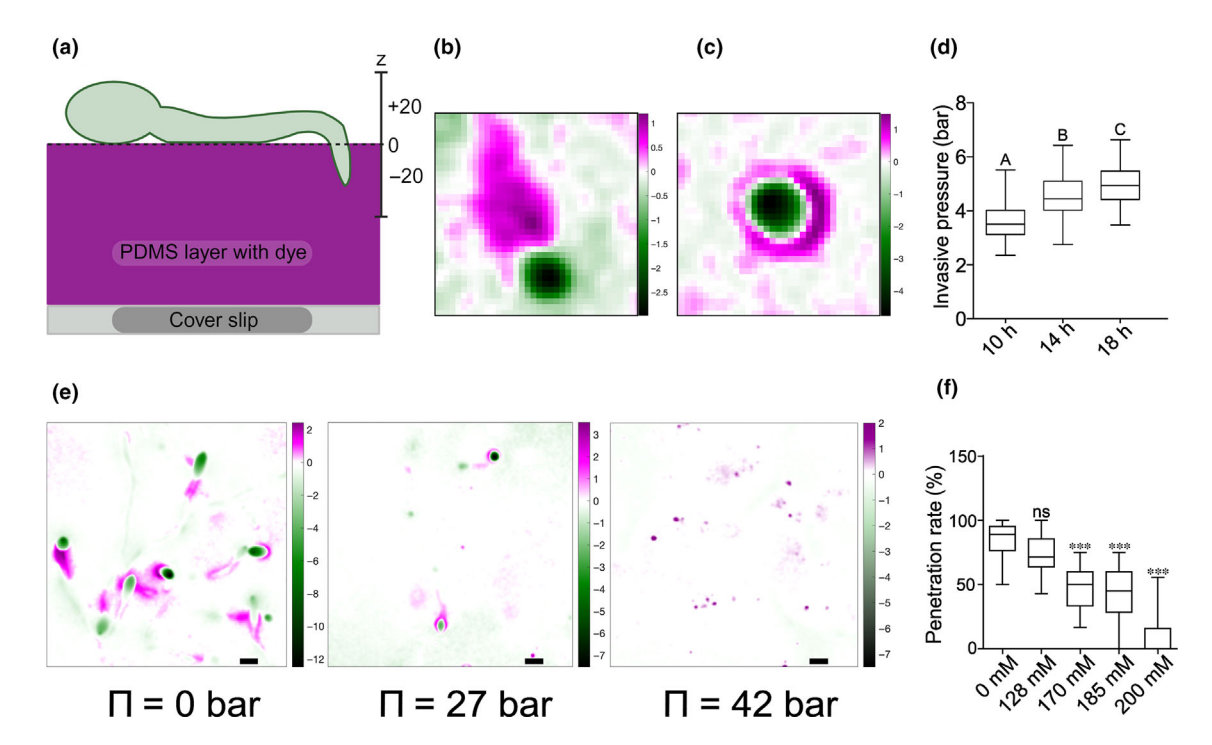


Fig. 3 Surface deformation maps of *Botrytis* on polydimethylsiloxane (PDMS) to calculate invasive and maximum turgor. (a) Model of the setup used to create surface deformation map. (b, c) Surface deformation maps after 10 h (b) and 18 h (c). Scale is in μ m. (d) Invasive pressure at 10 h (n = 50), 14 h (n = 61) and 18 h (n = 51). Box limits represent the 25^{th} – 75^{th} percentile, the horizontal line the median and the whiskers minimum to maximum values. Significant differences were analysed by one-way ANOVA with the Tukey *post hoc* test. Different letters indicate significant differences; P < 0.01. Raw data are found in Supporting Information Table S3. (e) Surface deformation maps of *Botrytis* on PDMS generating an osmotic counter pressure via the addition of different PEG2000 concentrations. (f) Box plot showing the relative amount of penetrations using 0 mM (n = 288), 85 mM (n = 28), 128 mM (n = 207), 170 mM (n = 102), 185 mM (n = 112) and 200 mM (n = 55) PEG2000. Box limits in the graph represent the 25^{th} – 75^{th} percentile, the horizontal line the median and the whiskers minimum to maximum values. Significant differences were analysed by one-way ANOVA with Dunnet *post hoc* test, ***, P < 0.001; ns, not significant. Experiments were repeated twice with similar results; representative surface deformation maps are shown. Raw data are found in Table S3.

previously established 12-fold mutant (12×bb) et al., 2022) and includes deletion of the two most abundant polygalacturonases (PG1 and PG2) as well as the recently discovered phytotoxic proteins, SSP2 (Zhu et al., 2022), Hip1 (Jeblick et al., 2023) and CDI1 (Zhu et al., 2023). The corresponding genes of many of them are expressed early during host infection (Müller et al., 2018), and we hypothesized that their function might directly impact on plant cell wall integrity (e.g. polygalacturonases, xylanases and a xyloglucanase), facilitating penetration. Thus, the 18-fold mutant allows to separate the mechanical part of the host infection from the biochemical part. In comparison with WT Botrytis, infection of the 18-fold mutant is strongly impaired in virulence as shown by significantly reduced lesions on tomato leaflets (Fig. 4e). To test whether this virulence reduction is related to invasive pressure generation, we again used fluorescently labelled PDMS in combination with confocal microscopy to determine the generated invasive pressure. However, in comparison with the WT, we did not find a reduction in pressure generation in the 18-fold mutant. In agreement, infection in the presence of 1 µM LatB was significantly reduced in 18-fold mutant and in the WT (Fig. S8), suggesting independent contributions of physical penetration and phytotoxic activity to the virulence of Botrytis.

Discussion

To overcome the external barriers of their hosts, necrotrophic fungi like Botrytis secrete a cocktail of cell wall degrading enzymes, cytolytic and phytotoxic proteins as well as different toxins (Bi et al., 2022). Together, this induces structural weakening of preformed barriers such as cuticle, cell wall and plasma membrane. This is a decisive difference in comparison to biotrophs, which use effectors to suppress plant defence responses but need to penetrate the fully intact plant barriers. Hence, high turgor pressure based on specialized appressoria is common in many biotrophs and hemi-biotrophs such as Blumeria graminis and Magnaporthe oryzae. By contrast, if the mechanical strength of the plant barriers is weakened by the secretion of the toxic cocktail from Botrytis, the question arises as to what extent the generation of turgor pressure is needed for the infection process of this model necrotroph. To address this quantitatively and mechanistically, we used an artificial substrate (PDMS), which mimics hydrophobicity and elasticity of plants leaves and has been used previously to investigate penetration mechanics of the oomycete *Phytophthora* (Bronkhorst *et al.*, 2021). The ability to neglect the phytotoxic and wall degrading activity of Botrytis renders PDMS an ideal tool to investigate turgor-driven penetration mechanics.

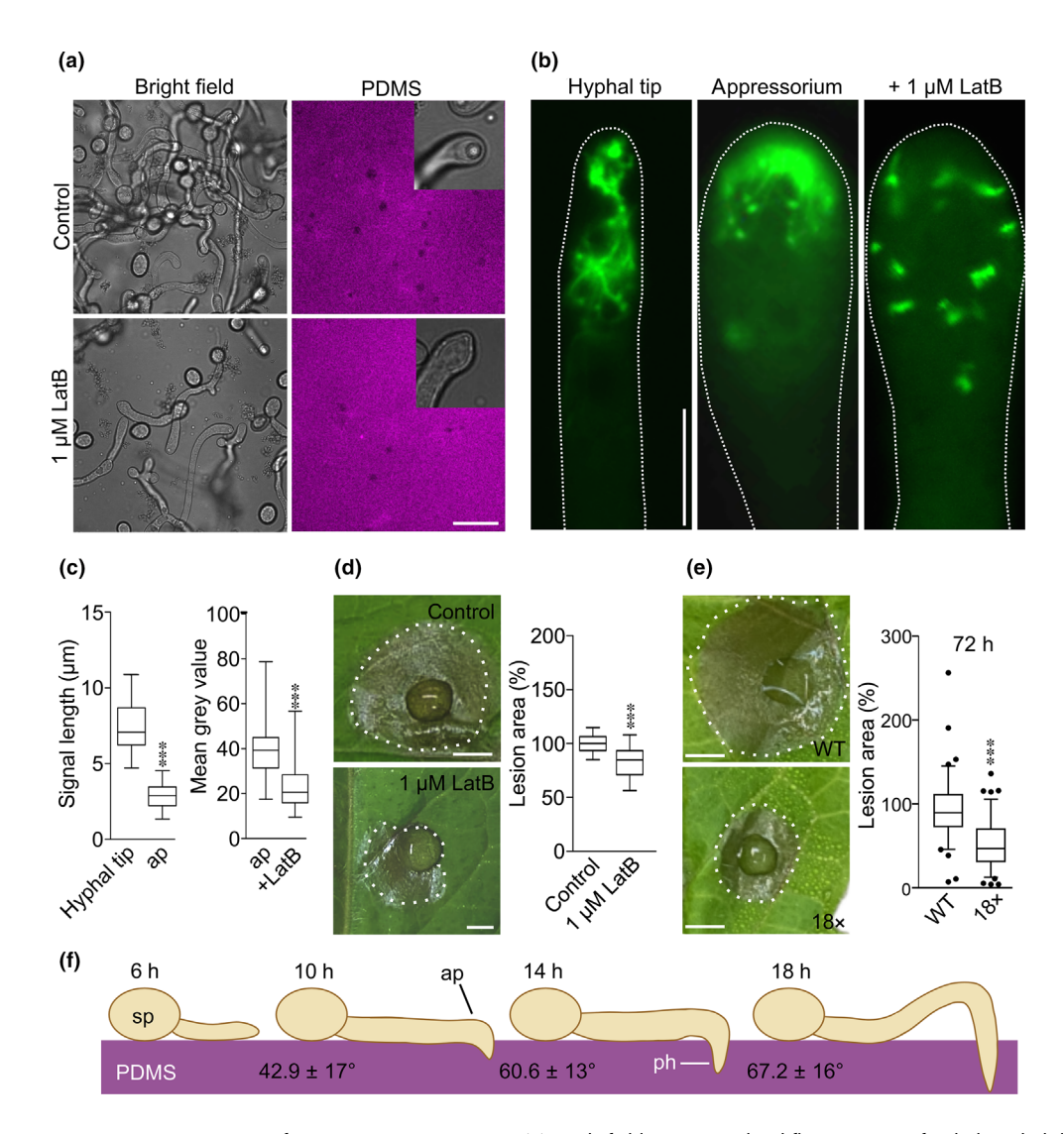


Fig. 4 Actin filament organization is prerequisite for penetration in *Botrytis*. (a) Brightfield images and red fluorescence of polydimethylsiloxane (PDMS) 8 h (18 h total) after adding latrunculin B (LatB) to a final concentration of 1 μM. Bar, 20 μm. (b) Visualization of the actin cytoskeleton using Lifeact-GFP in tips of growing hyphae, appressoria and upon 1 μM LatB treatment. Upon appressorium formation, actin signals condensate at the very tip of the hypha. Bar, 5 μm. (c) Quantification of signal length comparing signal distribution in the hyphal tip and the appressorium (n = 7 and n = 13) as well as quantification of fluorescence intensity of the appressorium in dependence of LatB (n = 13 and n = 10). Box limits represent the 25th–75th percentile, the horizontal line the median and the whiskers minimum to maximum values. To analyse statistical differences, a Student t-test was carried out; ****, P < 0.001. (d) Infection test of wild-type (WT) *Botrytis* B05.10 in presence of 0 mM (n = 54) and 1 μM (n = 27) latrunculin B on tomato leaflets after 72 h. Box plot showing the relative necrotic area with the WT mean set to 100%. Box limits in the graph represent the 25th–75th percentile, the horizontal line the median and whiskers 10–90%. Putative differences were analysed by one-way ANOVA with Dunnett's *post hoc* test (control: 0 Mm LatB), ****, P < 0.001; ns, not significant. Bars, 4 mm. (e) Infection test of WT *Botrytis* (n = 48) and the 18-fold (18x) mutant (n = 48) on tomato leaflets after 72 h. Box plot showing the relative necrotic area with the WT mean set to 100%. Box limits in the graph represent the 25th–75th percentile, the horizontal line the median and whiskers 10–90% with dots being values outside of that range. Putative differences were analysed by one-way ANOVA with Dunnett's *post hoc* test (control: WT), ****, P < 0.001. Experiments were repeated twice with similar results. Bars, 4 mm. Raw data for (c) and (e) are found in Supporting Information Tab

Our data reveal a unique and time-dependent penetration pattern by *Botrytis* on PDMS (Fig. 4f). Notably, using Arabidopsis as host we do observe similar penetration patterns in individual events (Fig. 1d), indicating that the findings on PDMS are not entirely artificial. 3D reconstructions of different stages of penetration displayed changing entry angles (Fig. 2). While initially, the penetration angle was oblique as reported for the *naifu*

penetration by *Phytophthora* (Bronkhorst *et al.*, 2021), later stages showed an increasingly perpendicular angle together with an arching of the fungal hypha above the site of penetration. This coincides with a change in adhesion pattern: whereas initially the area of adhesion is comet-shaped before the penetration site, resembling the *naifu* penetration once more, in later stages additional adhesion zones surrounding the invasion sites were

detected. The emerging adhesion pattern is a concentric isotropic adhesion area around the indentation as expected for a typical appressorium. Since zones of adherence were positive for concanavalin A, carbohydrate-binding could be involved in *Botrytis* surface attachment. This transition in adhesion pattern might also explain the initially observed changes in penetration angle, and together fit well with the observed unique penetration pattern.

Previously, reinforcing the appressorium wall by melanin was believed to be the prerequisite for the generation of high invasive pressures. Nevertheless, for the necrotrophic fungus Sclerotinia sclerotiorum, cuticle indentation has been observed (Lumsden & Wergin, 1980), supporting the necessity of mechanical force for infection. Based on electron microscopical studies, however, it was observed that the penetration peg of Sclerotinia had only a thin layer of cell wall which was thought to be insufficient to hold high pressure (Tariq & Jeffries, 1986). Following this evidence, it was assumed until recently that enzymatic activities were more important for appressorium-mediated penetration of Sclerotinia (Liang & Rollins, 2018). Based on the contact-mechanics model described previously (Bronkhorst et al., 2021), we calculated the invasive pressure of Botrytis at different stages of penetration. In accordance with the initial polarized mechanical geometry and the occurrence of a more concentric circular symmetry later, the invasive pressure was increased from 3.7 to 5.0 bar within 8 h (Fig. 3). A reason for the only moderate increase in pressure might be the nonsynchronized fungal penetration of PDMS. The occurrence of different stages at the same time is indicated by the relatively broad distribution of pressures at the single time points. The calculated maximal turgor pressure of >40 bar for *Botrytis* is well within the reported values for (hemi-) biotrophic fungi, which form specialized appressoria (Bechinger et al., 1999; Loehrer et al., 2014).

Our results show that for Botrytis, the generation of pressure and subsequent penetration is dependent on functionality of the actin cytoskeleton (Fig. 4). Recently, this has been also reported for Phytophthora and Colletotrichum (Bronkhorst et al., 2021, 2022; Zhang et al., 2022), indicating a conserved role of actin for appressorium development. In line with this, pharmacological interference of actin polymerization by LatB did affect the Botrytis appressorium formation and subsequently impacted penetration as well as virulence. However, it is unclear how the cytoskeleton precisely contributes to the translation of generated turgor pressure into physical (invasive) force. It has been speculated that actin filaments in the hyphal tip of *Phytophthora* serve as 'mechanostat' to sense and react to mechanical stress. According to the authors, cytoskeletal stiffness is adapted to the level of stress exerted on the hyphal tip to ensure sufficient rigidity during invasion (Bronkhorst et al., 2022). Another possible contribution of the cytoskeleton to physical force generation might be the direction of uniform turgor pressure towards the future penetration site. In M. oryzae an actin network is formed at the base of the appressorium at the point where the penetration peg will emerge (Dagdas et al., 2012). Together with guanosine triphosphatases, so-called septins, a ring structure is formed which provides the cortical rigidity channelling the osmotic pressure to generate physical force applied by the penetration peg (Dagdas et al., 2012). In line with this, the semi-to-full circular

assembly of actin signals during appressorium formation in Botrytis (Fig. 4b) is reminiscent of the toroidal-shaped actin network in M. oryzae. Here, septins form a scaffold for the organization of filamentous actin, and a septin knockout leads to cytoskeletal disorganization, preventing the penetration peg to be formed and eventually rendering the septin null mutants nonpathogenic (Dagdas et al., 2012). The only characterized septin homologue in Botrytis, Sep4, forms part of the diffusion barrier necessary for melanin and chitin accumulation in hyphal tips, participates in initiating the formation of infection structures and has been shown to be a virulence factor (Feng et al., 2017). Since they are highly conserved in filamentous fungi, it is conceivable, that septins in Botrytis recruit actin filaments in a similar manner as in M. oryzae appressoria (Eisermann et al., 2023). Another conserved and important class of proteins for appressorium formation are the so-called tetraspanins. In M. grisea, the tetraspanin MgPls1 is crucial for appressoriummediated penetration of host leaves (Clergeot et al., 2001). Orthologues of MgPLS1 have been found to be required for appressorial function and successful host penetration in several plant pathogenic fungi (Veneault-Fourrey et al., 2006). In Botrytis, a BcPLS1 null mutant was nonpathogenic on intact leaves but still able to infect wounded plant tissue (Gourgues et al., 2004).

To differentiate between the role of turgor pressure formation and secretion of proteins for virulence, we included a 18-fold *Botrytis* mutant, lacking most of the currently known phytotoxic proteins, in our study. Analysis of invasive pressure as well as exogenous application of LatB revealed a similar behaviour of *Botrytis* WT and the 18-fold mutant, which indicates at least partial independence of surface penetration by brute force and facilitated host infection through secretion of phytotoxic and cell wall degrading enzymes. Taken together, our data show that the necrotrophic fungus *Botrytis* uses actin-dependent turgor generation and surface adherence to employ a unique penetration pattern which contributes to overcome host resistance.

Acknowledgements

This work was supported by grants from the *BioComp* research initiative (Rhineland-Palatinate, Germany) and the German research foundation (DFG; SCHE 1836/5-1) to DS. JS and JB are supported by an ERC CoG grant, grant no. 101000981. Open Access funding enabled and organized by Projekt DEAL.

Competing interests

None declared.

Author contributions

TM performed most experiments. JM performed confocal microscopy. JB and JS calculated invasive and maximum pressure and provided surface deformation maps. NS and MH established the 18-fold *Botrytis* knockout mutant. TM, JS and DS designed the figures and performed statistical analysis. DS conceived the study and wrote the manuscript. All authors saw and commented on the manuscript.

ORCID

Jochem Bronkhorst https://orcid.org/0000-0002-8179-1099
Matthias Hahn https://orcid.org/0000-0002-5213-9034
Jonas Müller https://orcid.org/0000-0003-3211-3096
Tobias Müller https://orcid.org/0009-0002-0607-8709
David Scheuring https://orcid.org/0000-0001-9048-3330
Joris Sprakel https://orcid.org/0000-0001-6532-4514

Data availability

The data that support the findings of this study are integrated in the main article, and raw data are provided in Table \$3.

References

- Bechinger C, Giebel KF, Schnell M, Leiderer P, Deising HB, Bastmeyer M. 1999. Optical measurements of invasive forces exerted by appressoria of a plant pathogenic fungus. *Science* 285: 1896–1899.
- Bi K, Liang Y, Mengiste T, Sharon A. 2022. Killing softly: a roadmap of *Botrytis cinerea* pathogenicity. *Trends in Plant Science* 28: 211–222.
- Bronkhorst J, Kasteel M, van Veen S, Clough JM, Kots K, Buijs J, van der Gucht J, Ketelaar T, Govers F, Sprakel J. 2021. A slicing mechanism facilitates host entry by plant-pathogenic Phytophthora. *Nature Microbiology* 6: 1000–1006.
- Bronkhorst J, Kots K, De JD, Kasteel M, van Boxmeer T, Joemmanbaks T, Govers F, van der Gucht J, Ketelaar T, Sprakel J. 2022. An Actin mechanostat ensures hyphal tip sharpness in *Phytophthora infestans* to achieve host penetration. *Science Advances* 8: eabo0875.
- Clergeot PH, Gourgues M, Cots J, Laurans F, Latorse MP, Pepin R, Tharreau D, Notteghem JL, Lebrun MH. 2001. PLS1, a gene encoding a tetraspanin-like protein, is required for penetration of rice leaf by the fungal pathogen *Magnaporthe grisea*. Proceedings of the National Academy of Sciences, USA 98: 6963–6968.
- Coué M, Brenner SL, Spector I, Korn ED. 1987. Inhibition of actin polymerization by latrunculin A. FEBS Letters 213: 316–318.
- Dagdas YF, Yoshino K, Dagdas G, Ryder LS, Bielska E, Steinberg G, Talbot NJ. 2012. Septin-mediated plant cell invasion by the rice blast fungus, *Magnaporthe oryzae. Science* 336: 1590–1595.
- Dulal N, Rogers A, Wang Y, Egan M. 2020. Dynamic assembly of a higher-order septin structure during appressorium morphogenesis by the rice blast fungus. Fungal Genetics and Biology 140: 103385.
- Dulal N, Rogers AM, Proko R, Bieger BD, Liyanage R, Krishnamurthi VR, Wang Y, Egan MJ. 2021. Turgor-dependent and coronin-mediated F-actin dynamics drive septin disc-to-ring remodeling in the blast fungus *Magnaporthe* oryzae. Journal of Cell Science 134: cs251298.
- Eisermann I, Garduño-Rosales M, Talbot NJ. 2023. The emerging role of septins in fungal pathogenesis. Cytoskeleton 80: 242–253.
- Elad Y, ed. 2007. Botrytis. Biology, pathology and control. Dordrecht, the Netherlands: Springer.
- Feng H-Q, Li G-H, Du S-W, Yang S, Li X-Q, De Figueiredo P, Qin Q-M. 2017. The septin protein Sep4 facilitates host infection by plant fungal pathogens via mediating initiation of infection structure formation. *Environmental Microbiology* 19: 1730–1749.
- Gourgues M, Brunet-Simon A, Lebrun M-H, Levis C. 2004. The tetraspanin BcPls1 is required for appressorium-mediated penetration of *Botrytis cinerea* into host plant leaves. *Molecular Microbiology* 51: 619–629.
- Hématy K, Cherk C, Somerville S. 2009. Host–pathogen warfare at the plant cell wall. *Current Opinion in Plant Biology* 12: 406–413.
- Howard RJ, Ferrari MA, Roach DH, Money NP. 1991. Penetration of hard substrates by a fungus employing enormous turgor pressures. Proceedings of the National Academy of Sciences, USA 88: 11281–11284.
- Hunter PR, Craddock CP, Di Benedetto S, Roberts LM, Frigerio L. 2007. Fluorescent reporter proteins for the tonoplast and the vacuolar lumen identify

- a single vacuolar compartment in Arabidopsis cells. *Plant Physiology* **145**: 1371–1382.
- Hyde GJ, Davies D, Perasso L, Cole L, Ashford AE. 1999. Microtubules, but not Actin microfilaments, regulate vacuole motility and morphology in hyphae of *Pisolithus tinctorius*. Cell Motility and the Cytoskeleton 42: 114–124.
- Jeblick T, Leisen T, Steidele CE, Albert I, Müller J, Kaiser S, Mahler F, Sommer F, Keller S, Hückelhoven R et al. 2023. Botrytis hypersensitive response inducing protein 1 triggers noncanonical PTI to induce plant cell death. Plant Physiology 191: 125–141.
- Ketelaar T, Meijer HJG, Spiekerman M, Weide R, Govers F. 2012. Effects of latrunculin B on the actin cytoskeleton and hyphal growth in *Phytophthora* infestans. Fungal Genetics and Biology 49: 1014–1022.
- Leisen T, Bietz F, Werner J, Wegner A, Schaffrath U, Scheuring D, Willmund F, Mosbach A, Scalliet G, Hahn M. 2020. CRISPR/Cas with ribonucleoprotein complexes and transiently selected telomere vectors allows highly efficient marker-free and multiple genome editing in *Botrytis cinerea*. *PLoS Pathogens* 16: e1008326.
- Leisen T, Werner J, Pattar P, Safari N, Ymeri E, Sommer F, Schroda M, Suárez I, Collado IG, Scheuring D *et al.* 2022. Multiple knockout mutants reveal a high redundancy of phytotoxic compounds contributing to necrotrophic pathogenesis of *Botrytis cinerea*. *PLoS Pathogens* 18: e1010367.
- Leroch M, Mernke D, Koppenhoefer D, Schneider P, Mosbach A, Doehlemann G, Hahn M. 2011. Living colors in the gray mold pathogen *Botrytis cinerea*: codon-optimized genes encoding green fluorescent protein and mCherry, which exhibit bright fluorescence. *Applied and Environmental Microbiology* 77: 2887–2897.
- Liang X, Rollins JA. 2018. Mechanisms of broad host range necrotrophic pathogenesis in Sclerotinia sclerotiorum. Phytopathology 108: 1128–1140.
- Loehrer M, Botterweck J, Jahnke J, Mahlmann DM, Gaetgens J, Oldiges M, Horbach R, Deising H, Schaffrath U. 2014. *In vivo* assessment by Mach-Zehnder double-beam interferometry of the invasive force exerted by the Asian soybean rust fungus (*Phakopsora pachyrhizi*). *New Phytologist* 203: 620–631.
- Lumsden RD, Wergin WP. 1980. Scanning-electron microscopy of infection of bean by species of Sclerotinia. Mycologia 72: 1200–1209.
- Mendgen K, Deising H. 1993. Infection structures of fungal plant pathogens a cytological and physiological evaluation. *New Phytologist* 124: 193–213.
- Mendgen K, Hahn M. 2002. Plant infection and the establishment of fungal biotrophy. *Trends in Plant Science* 7: 352–356.
- Miyoshi M. 1895. Die Durchbohrung von Membranen durch Pilzfäden. *Jahrbucher fur Wissenschaftliche Botanik* 28: 269–289.
- Money NP. 1989. Osmotic pressure of aqueous polyethylene glycols: relationship between molecular weight and vapor pressure deficit. *Plant Physiology* 91: 766–769
- Money NP. 1995. Turgor pressure and the mechanics of fungal penetration. *Canadian Journal of Botany* 73: 96–102.
- Müller N, Leroch M, Schumacher J, Zimmer D, Könnel A, Klug K, Leisen T, Scheuring D, Sommer F, Mühlhaus T et al. 2018. Investigations on VELVET regulatory mutants confirm the role of host tissue acidification and secretion of proteins in the pathogenesis of *Botrytis cinerea*. New Phytologist 219: 1062–1074.
- Schumacher J. 2012. Tools for Botrytis cinerea: new expression vectors make the gray mold fungus more accessible to cell biology approaches. Fungal Genetics and Biology 49: 483–497.
- Talbot NJ. 2019. Appressoria. Current Biology 29: R144–R146.
 Tariq VN, Jeffries P. 1986. Ultrastructure of penetration of Phaseolus spp. by Sclerotinia sclerotiorum. Canadian Journal of Botany 64: 2909–2915.
- Vangalis V, Knop M, Typas MA, Papaioannou IA. 2021. Establishment of conidial fusion in the asexual fungus *Verticillium dahliae* as a useful system for the study of non-sexual genetic interactions. *Current Genetics* 67: 471–485.
- Veneault-Fourrey C, Lambou K, Lebrun M-H. 2006. Fungal Pls1 tetraspanins as key factors of penetration into host plants: a role in re-establishing polarized growth in the appressorium? FEMS Microbiology Letters 256: 179–184.
- Zhang Y, An B, Wang W, Zhang B, He C, Luo H, Wang Q. 2022. Actin-bundling protein fimbrin regulates pathogenicity via organizing F-actin dynamics during appressorium development in *Colletotrichum gloeosporioides*. *Molecular Plant Pathology* 23: 1472–1486.

Bedrijf, Wiley Online Library on [16/09/2024]. See the Term

Zhu W, Yu M, Xu R, Bi K, Yu S, Xiong C, Liu Z, Sharon A, Jiang D, Wu M et al. 2022. Botrytis cinerea BcSSP2 protein is a late infection phase, cytotoxic effector. Environmental Microbiology 24: 3420–3435.

Supporting Information

Additional Supporting Information may be found online in the Supporting Information section at the end of the article.

- Fig. S1 Botrytis development on glass.
- Fig. S2 Occurrence of infection hyphae on PDMS.
- Fig. S3 Comparison of wild-type Botrytis and Bcgfp1 infection.
- Fig. S4 Fitting intensity profiles to a sigmoidal function.
- Fig. S5 Fluorescent labelling of carbohydrates by concanavalin A.

- **Fig. S6** *Botrytis* germination and germ tube length in the presence of LatB.
- **Fig. S7** *Botrytis* infection, germination and germ tube length in the presence of oryzalin.
- Fig. S8 Infection of WT and 18-fold mutant in the presence of LatB.
- Table S1 Knockout genes of the Botrytis 18-fold mutant.
- **Table S2** gRNAs used for CRISPR/Cas9-mediated gene knock-out.
- Table S3 Raw data for the main figures.

Please note: Wiley is not responsible for the content or functionality of any Supporting Information supplied by the authors. Any queries (other than missing material) should be directed to the *New Phytologist* Central Office.